COMPUTING IDEAL MAGNETOHYDRODYNAMIC EQUILIBRIA

R. Keppens & J.W.S. Blokland
FOM Institute for Plasma Physics Rijnhuizen, Association Euratom-FOM
P.O. Box 1207, 3430 BE Nieuwegein, The Netherlands

I. INTRODUCTION

Nuclear fusion research promises to harvest the excess energy carried by energetic neutrons when Deuterium and Tritium hydrogen isotopes are fused together to form α-particles. Pressure and density conditions needed for these fusion reactions ensure that these charged constituents, together with the free electrons, form a fully ionized plasma at temperatures of about 100 million Kelvin. Any contact with material walls would instantaneously cool the plasma and must be avoided. In the axisymmetric toroidal vessel of a tokamak, a hot plasma is confined primarily by magnetic Lorentz forces. Strong helical magnetic fields that trace out nested toroidal surfaces help to thermally insulate the plasma from the walls and support it against its own pressure gradient. To lowest order, a fluid model of the equilibrium considers only this force balance in the poloidal cross-section of the tokamak, as expressed analytically by the Grad-Shafranov equation.

In this lecture, we discuss magnetohydrodynamic equilibria in general terms. For the static axisymmetric Grad-Shafranov case, a well-known analytic solution is presented. A proven numerical strategy for solving the Grad-Shafranov equation is given in some detail, and we discuss how generalizations (including equilibrium rotation, gravitation) from the static Grad-Shafranov case can be incorporated.

II. MAGNETOHYDRODYNAMIC EQUILIBRIA

A. Stationary MHD

The ideal magnetohydrodynamic (MHD) equations express conservation of mass, momentum, energy (internal + kinetic + magnetic), together with conservation of magnetic flux. For a vector magnetic field $\mathbf{B}$, fieldlines that are everywhere tangent to the local $\mathbf{B}$ can be introduced. The flux through an arbitrary surface intersecting a 'flux tube' bounded by fieldlines is $\Psi \equiv \int_S \mathbf{B}\cdot d\mathbf{S}$. Since the magnetic field obeys Maxwell's law $\nabla\cdot\mathbf{B} = 0$, it is easily seen that this is a meaningful quantity, as its value is identical for all cross-sectional surfaces along the flux tube. Indeed, apply Gauss theorem to the configuration in Figure 1 to find

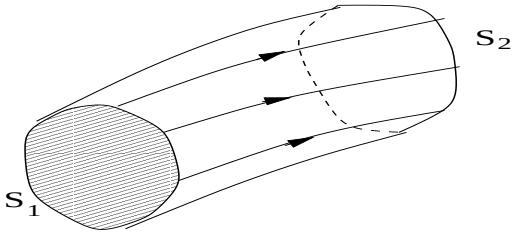

Figure 1: The magnetic flux through arbitrary cross-sections S_1 and S_2 of a flux tube bounded by magnetic fieldlines is identical.

$$\begin{aligned}\int_V \nabla\cdot\mathbf{B}\, dV &= -\int_{S_1}\mathbf{B}_1\cdot d\mathbf{S}_1 + \int_{S_2}\mathbf{B}_2\cdot d\mathbf{S}_2\\ &= 0.\end{aligned}$$

The basic law of ideal MHD expresses that magnetic flux is conserved in an even more general way: the flux through a co-moving surface element will remain constant, i.e. $\Psi = \int_C \mathbf{B}\cdot\mathbf{n}d\sigma =$ constant for any closed contour C moving with the plasma.

The conservation laws of ideal MHD form a set of 8 non-linear partial differential equations, with the magnetic field constrained 'topologically', by the non-existence of magnetic monopoles (Maxwell's law states that fieldlines have no beginning, nor end). For the computation of MHD equilibria, we seek time-invariant solutions of the following equations (see e.g. [11]):

$$\begin{aligned}\nabla\cdot(\rho\mathbf{v}) &= 0\\ \rho(\mathbf{v}\cdot\nabla)\mathbf{v} &= -\nabla p + (\nabla\times\mathbf{B})\times\mathbf{B} + \rho\mathbf{g}\\ (\mathbf{v}\cdot\nabla)p &= -\gamma p\nabla\cdot\mathbf{v}\\ \nabla\times(\mathbf{v}\times\mathbf{B}) &= 0\\ &\text{and}\quad \nabla\cdot\mathbf{B} = 0.\end{aligned}$$

In the above, we kept the possible influence of an external given gravitational field $\mathbf{g}$. Stationary solutions require to determine the spatial (3D) variation of density ρ, plasma flow $\mathbf{v}$, pressure p, and magnetic field $\mathbf{B}$. The parameter γ is the ratio of specific heats, for

an ideal gas $\gamma = 5/3$, and magnetic units have been adopted where the magnetic permeability $\mu_0 = 1$.

B. 2D stationary equilibria

Determining solutions to the (still) nonlinear partial differential equations is a formidable task. Restricting to essentially 2D solutions can be done by assuming a certain symmetry, like translational or axi-symmetry. It is then common to introduce a poloidal flux function ψ to obey the solenoidal constraint on $\mathbf{B}$ and thus set

$$\mathbf{B} = \hat{e}_z \times \nabla\psi + B_z \hat{e}_z, \quad \text{[translation]}$$

$$\mathbf{B} = \frac{1}{R}\hat{e}_\varphi \times \nabla\psi + B_\varphi \hat{e}_\varphi. \quad \text{[axisymmetry]}$$

The translational case is in a Cartesian (x, y, z) coordinate system, and for the axisymmetric case, we will consistently use a right-handed system (R, Z, φ). For nested flux surfaces where $\psi = 0$ is the magnetic axis, the function ψ is directly measuring the poloidal flux through a horizontal ribbon between the axis and the flux surface ψ hence

$$\int_{\psi=0}^{\psi} \mathbf{B}_p \cdot d\mathbf{S} \propto \psi.$$

The equilibrium problem can then be reformulated as a second order partial differential equation (PDE) for ψ, which in essence describes the force balance across flux surfaces (of constant ψ). Even then, the consistent incorporation of a stationary flow $\mathbf{v}_p$ in the 'poloidal' plane (x, y or R, Z) renders the problem mathematically complex. Indeed, depending on the (squared) local poloidal Alfvén Mach number defined as $M^2 = v_p^2/v_{A,p}^2 = \rho v_p^2/B_p^2$, the flow can change character from elliptic to hyperbolic [9, 10, 16]. We first discuss cases where poloidal flows are neglected, such that the governing PDE is always elliptic.

III. THE STATIC AXISYMMETRIC CASE

When static ($\mathbf{v} = 0$) solutions are sought, the problem becomes much more tractable, as we deal with force balance alone. In the axisymmetric case $\partial\varphi = 0$, we need to determine still 5 two-dimensional functions $\rho(R, Z)$, $p(R, Z)$, $B_R(R, Z)$, $B_Z(R, Z)$, and $B_\varphi(R, Z)$. Neglecting gravity, the density ρ is arbitrary, and the equilibrium problem merely balances pressure gradients with the Lorentz force, $\nabla p = (\nabla \times \mathbf{B}) \times \mathbf{B}$. Similar to the magnetic flux function ψ, a current stream function I is introduced with $\mathbf{J} = \nabla \times \mathbf{B} = -\frac{1}{R}\hat{e}_\varphi \times \nabla I + J_\varphi \hat{e}_\varphi$ (since also $\nabla \cdot \mathbf{J} = 0$). It is then easy to show that necessarily the pressure p is $p(\psi)$ and $I(\psi) = RB_\varphi$, and the governing Grad-Shafranov equation for ψ reads

$$R\frac{\partial}{\partial R}\left(\frac{1}{R}\frac{\partial\psi}{\partial R}\right) + \frac{\partial^2\psi}{\partial Z^2} = -I\frac{d\,I}{d\psi} - \frac{d\,p}{d\psi}R^2 = RJ_\varphi.$$

This must be solved for $\psi(R, Z)$ under a given $p(\psi)$ and $I(\psi)$. The Grad-Shafranov PDE is always elliptic, so that when formulated as a boundary value problem it is mathematically well-posed and the solution will reach its extremum on the boundary. In the context of fusion-relevant plasmas, the task to reconstruct the static MHD equilibrium configuration is to exploit the freedom in $p(\psi)$ and $I(\psi)$ to match measured profiles and/or global plasma parameters (like the total current or average gas to magnetic pressure ratios, etc.).

An important flux function which can be computed once a solution of the Grad-Shafranov equation is obtained is the $q(\psi)$ profile, which quantifies the change in toroidal angle $\Delta\varphi$ traversed as a magnetic field line wraps once around a full poloidal cross-section. Introducing poloidal polar coordinates (r, θ) centered on the major radius R_0 hence $R = R_0 + r\cos\theta$ and $Z = r\sin\theta$, field line trajectories are given by $Rd\varphi/B_\varphi = d\,r/B_r = r\,d\theta/B_\theta = d\,l/B_p$. Note that poloidal flux contours of constant $\psi(r, \theta)$ have arc length $dl = \sqrt{(}dr^2 + r^2 d\theta^2)$. The poloidal field is given by $B_p = \sqrt{(}B_r^2 + B_\theta^2) = \sqrt{(}B_R^2 + B_Z^2) = \mid \nabla\psi \mid /R$. Then

$$q(\psi) = \frac{\Delta\varphi}{\Delta\theta} = \frac{1}{2\pi}\int_0^{2\pi}\left(\frac{B_\varphi r}{RB_\theta}\right)_S d\theta,$$

where the integrand is evaluated on a constant flux surface S (see e.g. [4]). This reworks to

$$q(\psi) = \frac{I(\psi)}{2\pi}\oint\frac{d\,l}{R \mid \nabla\psi \mid} = \frac{1}{2\pi}\oint\frac{B_\varphi}{RB_p}d\,l.$$

The integral is now taken in the poloidal plane, along a poloidal flux contour. This 'safety factor' profile plays an important role for stability analysis.

A. Scaling for tokamak equilibria

When we want to determine a solution of the Grad-Shafranov equation within a given fixed cross-sectional boundary, taken to be a flux contour $\psi = \psi_1$, it is convenient computationally to exploit a scaling such that both flux values and coordinates become of unit range. For a tokamak with minor radius a and major radius R_0, the flux on the outer boundary ψ_1, together with the vacuum field B_0 at R_0, introduce

- a unit flux label $\bar{\psi} = \psi/\psi_1$
- the 'inverse flux' parameter $\alpha \equiv a^2 B_0/\psi_1$
- scaled poloidal coordinates $(x, y) \equiv (\frac{R-R_0}{a}, \frac{Z}{a})$.

When one also seperates the freedom in the arbitrary flux functions in terms of a (relative) amplitude A (B) and unit profile [5, 7], the core form of the Grad-Shafranov equation becomes

$$\frac{\partial^2\bar{\psi}}{\partial x^2} - \frac{\epsilon}{1+\epsilon x}\frac{\partial\bar{\psi}}{\partial x} + \frac{\partial^2\bar{\psi}}{\partial y^2} = A\left[\Gamma(\bar{\psi}) + Bx(1+\frac{\epsilon x}{2})\Pi(\bar{\psi})\right].$$

Here, the parameter $\epsilon = a/R_0$ is the inverse aspect ratio, and the unit profiles Γ and Π have $\Gamma(0) = 1$ and $\Pi(0) = 1$ and relate to the current and pressure gradient. In this formulation, the boundary conditions are: $\bar{\psi} = 1$ on the given boundary, and $\bar{\psi} = \bar{\psi}_x = \bar{\psi}_y = 0$ at the magnetic axis at $(x, y) = (\delta, 0)$. For the second order PDE, these 4 boundary conditions overdetermine the problem, rendering the determination of the amplitude A an integral part of the solution procedure (and the relative amplitude B too when the position of the magnetic axis δ is held fixed as well). Once the solution $\bar{\psi}$, A (and B) is identified for given functional profiles Γ and Π, we can compute the primitive variables

$$p/B_0^2 = \frac{\epsilon}{\alpha^2} \int^{\bar{\psi}} \left(-\frac{1}{2} AB\Pi \right) d\bar{\psi},$$

$$B_R/B_0 = -\frac{1}{\alpha} \frac{\epsilon}{1+\epsilon x} \frac{\partial \bar{\psi}}{\partial y},$$

$$B_Z/B_0 = \frac{1}{\alpha} \frac{\epsilon}{1+\epsilon x} \frac{\partial \bar{\psi}}{\partial x},$$

and

$$B_\varphi/B_0 = \frac{1}{1+\epsilon x} \left[1 - 2\frac{\epsilon}{\alpha^2} \int^{\bar{\psi}} A(\epsilon\Gamma - \frac{1}{2} B\Pi) d\bar{\psi} \right]^{1/2}.$$

Note that α does not appear in the governing equation, but it scales the obtained solutions, giving a different equilibrium realization for different α.

B. Solov'ev solution

An analytic solution to the Grad-Shafranov equation was given by Solov'ev [19]. In this case the right hand side of the Grad-Shafranov equation becomes independent of ψ by choosing linear profiles $I^2/2 = I_0^2/2 - E\psi$ and $p = p_0 - F\psi$ where E, and F are free profile parameters. A polynomial solution to the equation (verify by inspection) is then

$$\psi = \left(C + DR^2 \right)^2 + \frac{1}{2} \left[E + \left(F - 8D^2 \right) R^2 \right] Z^2,$$

where two integration constants C, D are introduced. It is instructive to change to the dimensionless $\bar{\psi}$ and (x, y) coordinates, and by redefining the integration constants rewrite the Solov'ev solution as

$$\bar{\psi} = \left[x - \frac{\epsilon}{2}(1 - x^2) \right]^2 + \left(1 - \frac{\epsilon^2}{4} \right) \left[1 + \tau\epsilon x(2 + \epsilon x) \right] \frac{y^2}{\sigma^2}.$$

The bounding unit $\bar{\psi} = 1$ contour goes through the 4 points $(x = \pm 1, y = 0)$ $(0, y = \pm\sigma)$, and τ measures the plasma triangularity (ellips-like for $\tau = 0$). Furthermore, $\bar{\psi} = 0$ at the magnetic axis $(\delta, 0)$ with

$$\delta = \frac{1}{\epsilon} \left[\sqrt{1 + \epsilon^2} - 1 \right],$$

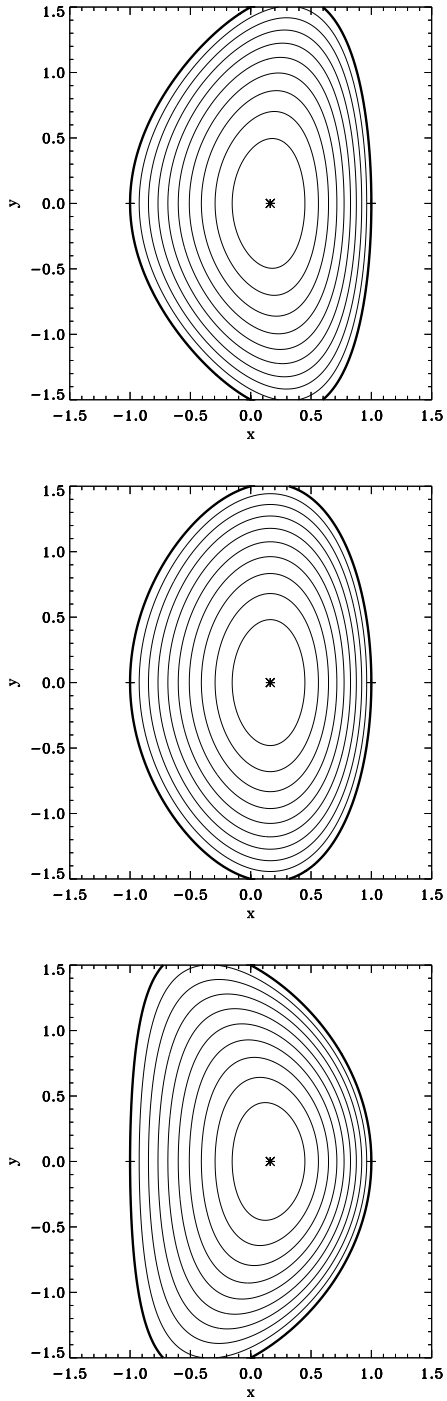

Figure 2: The analytic Solov'ev solution showing the plasma cross-sectional shape for fixed inverse aspect ratio $\epsilon = 1/3$, $\sigma = 1.5$ and varying triangularity $\tau = -0.5, 0, 0.5$ (top to bottom).

quantifying the outward Shafranov shift of the magnetic axis, a geometric effect required for equilibrium in a torus geometry. We can deduce that in terms of the unit profiles and amplitudes (eigenvalues), this solution has $\Gamma = 1 = \Pi$ with $A = \frac{2}{\sigma^2}\left(1 - \frac{\epsilon^2}{4} + \sigma^2\right)$ and $B = 2\epsilon\left(\tau(1 - \frac{\epsilon^2}{4}) + \sigma^2\right) / \left(1 - \frac{\epsilon^2}{4} + \sigma^2\right)$. As an example, Figure 2 shows the solution and the plasma cross-section for a case with inverse aspect ratio $\epsilon = 1/3$, $\sigma = 1.5$ and triangularity varied from $\tau = -0.5$, $\tau = 0$, to $\tau = 1.5$. Clearly, the triangular shape of the plasma cross-section enters as τ differs from zero, and its sign determines the orientation of the D-shape pattern. This analytic solution can be used to test numerical equilibrium codes, but it avoids the complications introduced by a nonlinear flux dependence of the right hand side RJ_φ.

IV. SOLVING GRAD-SHAFRANOV

In this section, we will discuss a particular numerical solution strategy for the Grad-Shafranov equation, where the plasma boundary shape is fixed and given a priori as a bounding flux contour. The discussion recalls the essential elements of proven implementations as found in [14, 2, 1, 18]. The emphasis is on computing the nested flux contours interior to this boundary to a high accuracy, ensuring among other things a continuous representation of $\bar{\psi}$ and $\nabla\bar{\psi}$. The core form of Grad-Shafranov can be written as

$$\Delta^*\bar{\psi} = F(\bar{\psi}),$$

where the non-linear $\bar{\psi}$ dependence is found in the right hand side. It is then convenient to use Picard iteration to converge on the solution, such that from a starting guess $\bar{\psi}^{(0)}(x, y)$, the iterate solves the linearized problem

$$\Delta^*\bar{\psi}^{(n+1)} = F(\bar{\psi}^{(n)}),$$

which is stopped when e.g. $\max |\ \bar{\psi}^{(n+1)} - \bar{\psi}^{(n)}\ | \leq \epsilon_{tol}$. The max-norm runs over all grid points, and tolerances ϵ_{tol} can be taken as low as 10^{-8} (depending on machine precision).

To further specify the solution algorithm, we need to explain the choice of the grid on which the solution is computed, the way in which the solution is approximated numerically on this grid, and the manner in which the PDE is turned into a discrete (linear algebraic) problem. A proven strategy which allows for a continuous $\nabla\bar{\psi}$ is to use a third order Finite Element method (FEM). On a unit square $[-1, 1]^2$, we can define up to 16 bicubic Hermite polynomials, 4 per corner $(x_0, y_0) = (\pm 1, \pm 1)$, namely

$$H_{00}(x, y) = \frac{1}{16}(x + x_0)^2(xx_0 - 2)(y + y_0)^2(yy_0 - 2),$$

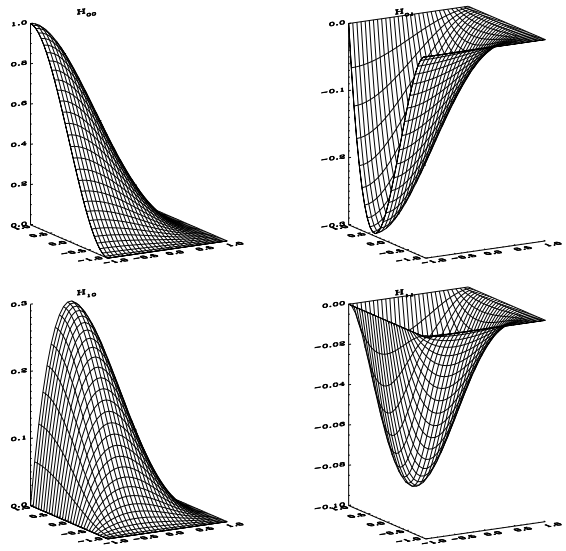

Figure 3: The bicubic Hermite elements as defined on a unit domain $[-1, 1]^2$.

$$H_{10}(x, y) = -\frac{1}{16}x_0(x + x_0)^2(xx_0 - 1)(y + y_0)^2(yy_0 - 2),$$

$$H_{01}(x, y) = -\frac{1}{16}(x + x_0)^2(xx_0 - 2)y_0(y + y_0)^2(yy_0 - 1),$$

$$H_{11}(x, y) = \frac{1}{16}x_0(x + x_0)^2(xx_0 - 1)y_0(y + y_0)^2(yy_0 - 1).$$

These elements for corner $(x_0, y_0) = (-1, 1)$ are shown in Figure 3. This allows to approximate any function $f(x, y)$ on $[-1, 1]^2$ by the expansion

$$\begin{aligned} f(x, y) = \quad & \textstyle\sum_{x_0,y_0} H_{00}(x, y)f(x_0, y_0) \\ & + H_{10}(x, y)\tfrac{\partial f}{\partial x}(x_0, y_0) + H_{01}(x, y)\tfrac{\partial f}{\partial y}(x_0, y_0) \\ & + H_{11}(x, y)\tfrac{\partial^2 f}{\partial y \partial x}(x_0, y_0) \end{aligned}$$

The function then has a prescribed functional dependence on the square as encoded in the bicubic expansion polynomials, and the 16 expansion coefficients are the local corner values of the function f and its derivatives.

For a given cross-sectional shape, the grid should allow alignment with the usually curved boundary. In the (x, y) plane, polar coordinates (r, θ) centered at $(x, y) = (0, 0)$ can be used to represent a given boundary curve in a (suitably truncated) Fourier series $a_B(\theta) = \sum_m a_m e^{im\theta}$. We can then use an arbitrary "radial" function $v(r)$ from 0 (center) to 1 (boundary) in global coordinates following the boundary shape where

$$x = v(r)a_B(\theta)\cos\theta, \quad y = v(r)a_B(\theta)\sin\theta.$$

Our grid is then formed by taken a discrete number n_r radial r_i and n_θ angular θ_j points. An example of such

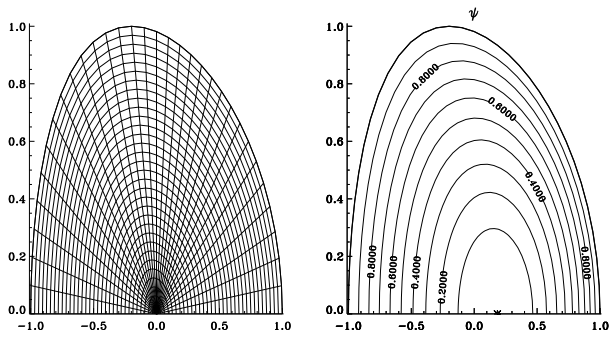

Figure 4: The computational grid (left) constructed to follow the boundary shape of a Solov'ev solution (right).

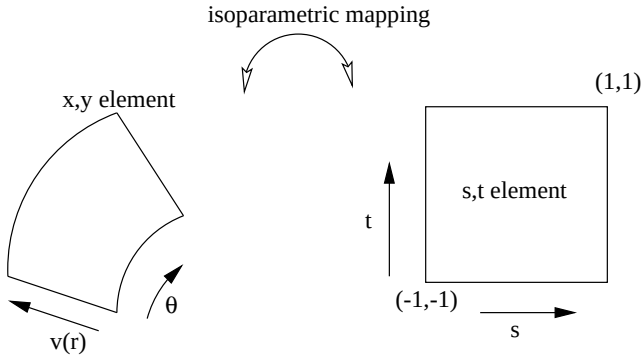

Figure 5: Isoparametric mapping to the local s,t coordinates for a curved quadrilateral on the square $[-1,1]^2$.

a grid is shown in Figure 4, the boundary of which corresponds to a Solov'ev equilibrium with $\epsilon = 0.38$, $\tau = 1$ and $\sigma = 0.98$. This grid consists of curved quadrilateral elements, while we discussed the FEM representation of a function on a unit element $[-1,1]^2$. The numerical representation of the solution on the boundary-fitted grid is complete by making use of an isoparametric mapping, where each curved quadrilateral is mapped on $[-1,1]^2$ by changing from (x,y) to local (s,t) coordinates (see Figure 5). In fact, this mapping consists of representing both the solution and the coordinates x, y in the same FEM representation, i.e.

$$\begin{aligned}
\bar{\psi}(x,y) = &\sum H_{00}(s,t)\bar{\psi}(s_0,t_0) + H_{10}(s,t)\frac{\partial\bar{\psi}}{\partial s}(s_0,t_0) \\
&+H_{01}(s,t)\frac{\partial\bar{\psi}}{\partial t}(s_0,t_0) + H_{11}(s,t)\frac{\partial^2\bar{\psi}}{\partial s\partial t}(s_0,t_0) \\
x(s,t) = &\sum H_{00}(s,t)x(s_0,t_0) + H_{10}(s,t)\frac{\partial x}{\partial s}(s_0,t_0) + \ldots \\
y(s,t) = &\sum H_{00}(s,t)y(s_0,t_0) + H_{10}(s,t)\frac{\partial y}{\partial s}(s_0,t_0) + \ldots
\end{aligned}$$

Identifying $v(r) \equiv s$ and $\theta \equiv t$, it is possible to compute the consistent FEM representation of the coordinates [as one can calculate x, $\partial x/\partial s$ etc. at all (s_0,t_0)]. One can use this flexibility (after each Picard iterate or after Picard convergence) to take the local s coordinate to become some function of $\bar{\psi}$, and align the grid with $\bar{\psi}$ flux contours.

Within each Picard step, one solves the discrete equivalent of $\Delta^*\bar{\psi}^{(n+1)} = F(\bar{\psi}^{(n)})$. In FEM methodology, we formulate the problem in its weak form, where we select a space of test-functions χ and look for the solution $\bar{\psi}$ such that for all test functions we have

$$\int_V \chi\nabla\cdot\left(\frac{1}{R^2}\nabla\bar{\psi}\right)dV = \int_V \chi\frac{F}{R^2}dV,$$

where the integral is taken over the plasma (tokamak) volume. In the Galerkin method, the test functions are simply the finite elements (H_{00} etc.) which are already used in the representation for ψ. This reduces the problem to a linear system $K\vec{x} = \vec{b}$, where the vector

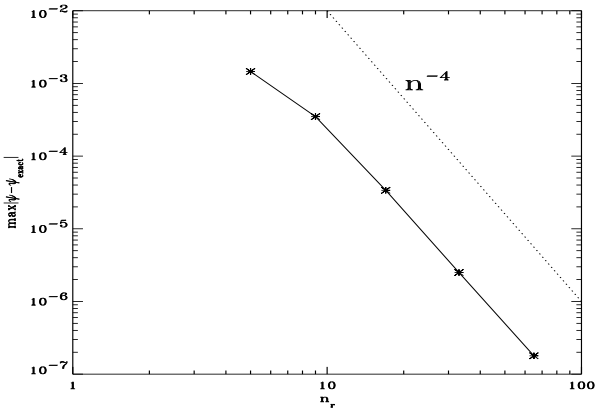

Figure 6: The fourth order convergence behavior as observed in the max-norm of the error in a computed Solov'ev equilibrium for increasing grid resolution.

$\vec{x}$ represents the unknown coefficients in the FEM representation, while the K matrix and $\vec{b}$ vector elements are integrals of known functions (involving the FEM and their derivatives). These integrals can e.g. be evaluated numerically by Gaussian quadrature. Figure 6 shows the expected quartic convergence reached when a Solov'ev solution is determined numerically for increasing grid resolution $n_r = n_\theta$ going from 5 up to 65. As the exact solution is known, the error can be quantified precisely and the fourth order convergence in $\bar{\psi}$ shows that very accurate solutions are already obtained for relatively coarse grids.

V. GENERALIZATIONS

A. Toroidal rotation

The purely static, axisymmetric, non-gravitating case can be generalized in several ways. Avoiding the

significant complications due to poloidal flow, a first non-trivial extension of the Grad-Shafranov equilibrium includes the effect of toroidal rotation and the associated centrifugal force. The toroidal component of the stationary induction equation $\nabla \times (\mathbf{v} \times \mathbf{B}) = 0$ then dictates that each flux surface rotates at fixed angular velocity $\Omega(\psi) = v_\varphi / R$.

The azimuthal component of the force balance equation still prescribes the current stream function I to be a flux function $I(\psi) = RB_\varphi$. However, the poloidal part now requires two equations to be satisfied simultaneously. In the $\nabla\psi$ direction, a Grad-Shafranov-like equation is obtained, namely

$$R\frac{\partial}{\partial R}\left(\frac{1}{R}\frac{\partial \psi}{\partial R}\right) + \frac{\partial^2 \psi}{\partial Z^2} = -I\frac{dI}{d\psi} - \frac{\partial p}{\partial \psi}R^2 = RJ_\varphi,$$

where the pressure is no longer a flux function. The dependency of the pressure $p(\psi, R)$ is such that along the poloidal flux contours the force balance is ensured [13] by

$$\frac{\partial p}{\partial R}_{|\,\psi} = \rho R\Omega^2(\psi).$$

The latter equation can, e.g. be solved analytically under the additional assumption that the entropy $S = p\rho^{-\gamma}$ is a flux function, a result which generalizes to all stationary MHD equilibria since $\mathbf{v} \cdot \nabla S = 0$ (with poloidal flows as well). The pressure can be written as

$$p(\psi, R) = \left[R^2 \frac{\gamma - 1}{\gamma}\frac{\Omega^2}{2S^{\frac{1}{\gamma}}} + f\right]^{\frac{\gamma}{\gamma - 1}}$$

so that for toroidally rotating equilibria four flux functions can be freely chosen: besides $I(\psi)$ and $\Omega(\psi)$ we get e.g. $S(\psi)$ and $f(\psi)$. For the purpose of equilibrium reconstruction for toroidally rotating tokamak plasmas where diagnostic information on density and temperature (hence pressure) profiles is available, a convenient parametrization uses the corresponding static pressure $p_{\rm st}(\psi)$ and density $\rho_{\rm st}(\psi)$ profiles with the same entropy variation $S(\psi)$ as follows:

$$p(\psi, R) = p_{\rm st}(\psi)\left[(R^2 - R_0^2)\frac{\gamma - 1}{\gamma}\frac{\Omega^2 \rho_{\rm st}}{2p_{\rm st}} + 1\right]^{\frac{\gamma}{\gamma - 1}}.$$

This is useful as long as the toroidal rotation is low and its small influence on the equilibrium properties is to be quantified in comparison with a similar static reconstruction. The pressure can be shown to have its maximum shifted radially outward with respect to the magnetic axis, which in turn is shifted outward due to toroidal rotation.

As an example, Figure 7 shows the influence of a relatively large toroidal rotation on the pressure profile. We considered a circular tokamak cross-section

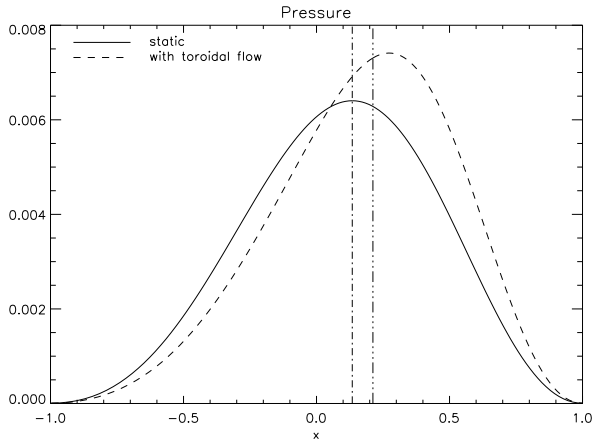

Figure 7: The radial pressure profile for a static and corresponding toroidally rotating equilibrium, with the free profiles chosen as indicated in the text. Note the outward shift of the magnetic axis (vertical dahsed lines), and the seperation of the pressure maximum from the magnetic axis when a (large) rotation is present.

of inverse aspect ratio $\epsilon = 0.26$ (as in the TEXTOR tokamak) and parametrized the various free profiles as follows

$$\begin{aligned} I^2 &= A\left[1 - 0.01\psi + 0.005\psi^2\right], \\ p_{\rm st} &= 0.0125\, A\left[1 - 2\psi + 1.001\psi^2\right], \\ \rho_{\rm st} &= A\left[1 - \psi + 0.6\psi^2 - 0.5\psi^4\right], \\ \Omega &= 0.075\left[1 - 0.999\psi\right], \end{aligned}$$

where the latter two only enter in the computation when rotation is considered. The eigenvalue A determined numerically is 164 in the static case, versus 155 for the rotating equilibrium. The rotation would correspond to a maximal sonic Mach number $M_s = v_\varphi / \sqrt{\gamma p/\rho} = 1.06$. This value is rather high (compare to a value of 0.24 reached at maximal Neutral Beam Injection power on the TEXTOR tokamak [3]), but illustrates well the influence of toroidal rotation. The vertical lines indicate the magnetic axis locations, and for this exaggerated rotation the pressure maximum clearly separates from the shifted magnetic axis.

B. Gravitating cases

Typical operational parameters for a tokamak consider a particle number density $n = 10^{20}$ m^{-3}, a magnetic field of $B = 3T$, and a temperature of 10^8 Kelvin. The ratio of Lorentz forces to the pressure gradient is of order of the inverse of the plasma beta $\beta = 2p/B^2$, a factor of 50. Estimating the role of subsonic toroidal rotation at sonic Mach $M_s = 0.25$ in a vessel with inverse aspect ratio $\epsilon = 0.3$, the pressure gradient is similarly outweighing the centrifugal force by about 50. The

earth's gravitational influence on the tokamak plasma can safely be neglected, as even the centrifugal force is dominating gravity by a factor of 10^{10}.

In astrophysical contexts, the influence of external or self-gravity can become very important in the overall force balance. In accretion disks for example, the pure Keplerian disk balances a central gravitational field with centrifugal forces. In the solar corona, quiescent prominences can be observed suspended above the solar limb, characterized by much denser and much cooler (typical factors 10-100) plasma than the coronal environment. There, the main force balance is again determined by Lorentz forces, now opposing gravity and pressure gradients. A recent analytical solution representative for quiescent prominences can be found in [17]. A similar analysis of the static force balance, now assuming translational invariance in the z-direction finds for force balance in the $\nabla\psi$ direction

$$\frac{\partial^2\psi}{\partial x^2}+\frac{\partial^2\psi}{\partial y^2}=-I\frac{d\,I}{d\,\psi}-\frac{\partial p}{\partial\psi}=J_z.$$

Again, $I(\psi)=B_z$ is a free flux function and $p(\psi,y)$. Along a poloidal flux contour the equation

$$\frac{\partial p}{\partial y}_{|\psi}=-\rho g$$

should be satisfied when considering a constant external gravitational acceleration $\mathbf{g}=-g\hat{e}_y$. Assuming the temperature to be a flux function $T(\psi)$, three free flux functions can be chosen as the pressure is then $p(\psi,y)=k(\psi)\exp(-g\,y/T(\psi))$. Using a scaling with respect to half the horizontal diameter a, the outermost flux value ψ_1 and a reference field strength B_0, a suitable scaling writes the governing Grad-Shafranov-like equation as

$$\frac{\partial^2\psi}{\partial x^2}+\frac{\partial^2\psi}{\partial y^2}=-\alpha^2\left[I\frac{d\,I}{d\,\psi}+\left(\frac{d\,l}{d\,\psi}+\frac{l\,y}{H^2}\frac{d\,H}{d\,\psi}\right)e^{-\frac{y}{H}}\right],$$

where $\alpha=a\,B_0/\psi_1$, and the pressure $p=l(\psi)e^{-\frac{y}{H}}$ uses the scale height $H=T(\psi)/(ag)$. All quantities appearing are again dimensionless, so e.g. $(x/a,(y-y_0)/a)\rightarrow(x,y)$ with y_0 a reference height in the prominence. The same numerical approach can be adopted to numerically compute these astrophysically relevant equilibria.

C. General case

Extending the computation of symmetric equilibria to cases where poloidal flows are allowed, without or with gravitational effects, introduces a stream function χ to obey mass conservation $\nabla\cdot(\rho\mathbf{v})=0$ in analogy with the magnetic flux function ψ. Poloidal flow streamlines and poloidal flux contours coincide as $\chi(\psi)$, and it can

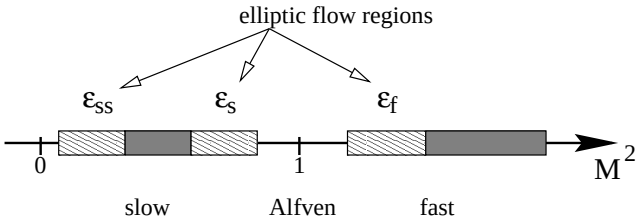

Figure 8: For stationary MHD equilibria with non-vanishing poloidal flows as measured by their squared poloidal Alfvén Mach number M^2, three elliptic flow regimes occur: subslow ϵ_{ss}, slow ϵ_s and fast ϵ_f.

be shown that all stationary equilibria follow from a variational principle [12]

$$\delta\int\left(\rho v_p^2+p-B_p^2/2+B_\varphi^2/2\right)dV=0.$$

The most suitable form to express the Lagrangian density (the integrand) for subsequent analysis rewrites it in terms of $(\psi,\nabla\psi,M^2)$ with the poloidal Alfvén Mach from $M^2=(d\chi/d\psi)^2/\rho$ [8]. The Euler-Lagrange equations then represent the generalization of the static symmetric equilibrium problem. Mathematically, the second order PDE governing force balance across flux surfaces is augmented with a nonlinear algebraic relation between M^2 and $(\psi,\nabla\psi)$. This Bernoulli law expresses energy conservation along a fieldline. The essential dependency $M^2(\psi,\mid\nabla\psi\mid^2)$ makes the character of the governing PDE for ψ dependent on M^2. It turns out that three elliptic flow regimes exist, with poloidal flow speeds either subslow [with squared $M^2<M_c^2=\gamma p/(\gamma p+B^2)$] , slow [sub-Alfvénic $M^2<1$] or fast [super-Alfvénic $M^2>1$]. Schematically indicated in Figure 8, these elliptic flow regimes are generally seperated by hyperbolic regimes, and reflect the intrinsic three-fold structure of MHD flows [6].

The methodology for computing the elliptic equilibrium problems neglecting poloidal flows can still be used, as long as a particular elliptic flow regime is preselected. This can be done since the roots of the algebraic Bernoulli expression can be bracketed according to the three elliptic flow regimes. A double iteration is then required, where in the outer loop, for given ψ values on the grid, the selected root of the Bernoulli equation determines all local M^2 values. The inner loop solves the then elliptic equilibrium PDE for ψ at the fixed M^2 values using the Picard iteration as before. The double iteration is then found to converge typically as shown in Fig. 9. Example equilibria for tokamak configurations as well as for accretion disk tori can be found in [1]. For cases when gravity, poloidal and toroidal flows are all present, a total of five free flux functions are to be specified, compared to the two flux functions arising in

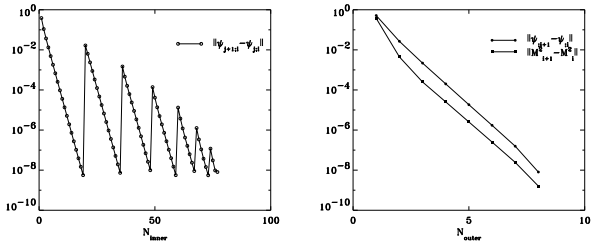

Figure 9: Representative convergence histories for the inner Picard iteration (left) and the outer iteration (right) on the combined Bernoulli-generalized Grad-Shafranov equilibrium problem in the presence of poloidal flows.

the standard Grad-Shafranov problem. In the context of tokamak equilibria, where gravity is negligible, still 4 profiles enter when poloidal flows are to be accounted for. A fifth one is needed if one wants to compute all primitive variables (ρ, p, $\mathbf{v}$, $\mathbf{B}$).

VI. CONCLUDING REMARKS

We discussed MHD equilibria in general terms, along with proven strategies employed to compute accurate 2D equilibria. The accuracy obtained by using bicubic finite elements for representing ψ is beneficial when the equilibria are to be analysed further for MHD stability against linear perturbations. The representation using isoparametric bicubic elements allows to compute the metric for the non-orthogonal coordinate system in which the fieldlines appear straight, and the equilibrium itself is obeyed to second order accuracy. These ingredients are then passed on to linear MHD solvers exploiting these coordinate systems to properly capture the wave polarizations [15].

In our description, we assumed a given fixed outer flux contour, and how elliptic solvers can be used to obtain the interior nested flux distribution. Note that the equilibrium problem in a tokamak can encompass plasma-vacuum-wall configurations, where the determination of the plasma-vacuum boundary turns the computation in a free boundary problem. Similarly, free-boundary problems generally prevail in solar prominences or astrophysical accretion disks. In tokamaks with a divertor, a magnetic separatrix bounds regions of nested and open flux surfaces (the Scrape-Off-Layer), introducing further complications for equilibrium reconstructions.

ACKNOWLEDGMENTS

This work is supported by the contract of Association between Euratom/FOM, within the framework of the European Fusion Programme. Opinions expressed herein do not necessarily reflect those of the EC.

REFERENCES

1. A.J.C. Beliën, M.A. Botchev, J.P. Goedbloed, B. van der Holst, R. Keppens, *JCP* **182**, 91 (2002)
2. A.J.C. Beliën, S. Poedts, J.P. Goedbloed, *Comp. Phys. Commun.* **106**, 21 (1997)
3. J.W.S. Blokland, R. Keppens, J.P. Goedbloed, R.J.E. Jaspers, M.F.M. de Bock, and the TEXTOR team, *Proc. EPS 2005*
4. J.P. Freidberg, *Ideal Magnetohydrodynamics* (Plenum Press, New York, 1987)
5. J.P. Goedbloed, *Comp. Phys. Commun.* **31**, 123 (1984)
6. J.P. Goedbloed, *Space Science Rev.* **107**, 353 (2003)
7. J.P. Goedbloed, *Transactions of fusion science and technology* **45**(2T), 79 (2004)
8. J.P. Goedbloed, *Phys. Plasmas* **11**(12), L81 (2004)
9. J.P. Goedbloed, A. Lifschitz, *Astrophys. Lett. and Communications* **34**, 261 (1996)
10. J.P. Goedbloed, A.E. Lifschitz, *Phys. Plasmas* **4**, 3544 (1997)
11. J.P. (Hans) Goedbloed, S. Poedts, *Principles of Magnetohydrodynamics*, Cambridge University Press, 2004
12. M. Heinemann, S. Olbert, *J. Geophys. Res.* **83**, 2457 (1978)
13. B. van der Holst, A.J.C. Beliën, J.P. Goedbloed, *Phys. Plasmas* **7**(10), 4208 (2000)
14. G.T.A. Huysmans, J.P. Goedbloed, W. Kerner, in: *Proc. CP90 Conf. on Comp. Phys. Proc.* (World Scientific Publ. Co., Singapore), 371 (1991)
15. W. Kerner, J.P. Goedbloed, G.T.A. Huysmans, S. Poedts, E. Schwarz, *J. Comput. Phys.* **142**, 271 (1998)
16. A.E. Lifschitz, J.P. Goedbloed, *J. Plasma Phys.* **58**, 61 (1997)
17. B.C. Low, M. Zhang, *Astropys. J.* **609**, 1098 (2004)
18. H. Lütjens, A. Bondeson, A. Roy, *Comp. Phys. Commun.* **69**, 287 (1992)
19. L.S. Solov'ev, *Sov. Phys.-JETP 26*, 400 (1968)